Microfluidic fuel cell based on laminar flow[☆]

Eric R. Choban[a,b], Larry J. Markoski[b], Andrzej Wieckowski[c], Paul J.A. Kenis[a,b,*]

[a] *Department of Chemical and Biomolecular Engineering, University of Illinois, 600 Mathews Avenue, Urbana, IL 61801, USA*
[b] *Beckman Institute of Advanced Science and Engineering, Urbana, IL 61801, USA*
[c] *Department of Chemistry, University of Illinois, Urbana, IL 61801, USA*

Abstract

This paper discusses a novel microfluidic fuel cell concept that utilizes the occurrence of multi-stream laminar flow at the microscale to keep the fuel and oxidant streams separated yet in diffusional contact. The system consists of a Y-shaped microfluidic channel in which two liquid streams containing fuel and oxidant merge and continue to flow laminarly in parallel between two catalyst-covered electrodes on opposing walls without turbulent mixing. Preliminary results indicate that this novel fuel cell concept may lead to the development of efficient room temperature power sources of microscopic dimensions that are comparable or better in performance than conventional polymer–electrolyte-membrane based microfuel cells that typically operate between 60 and 80 °C.
© 2004 Elsevier B.V. All rights reserved.

Keywords: Microfluidics; Laminar flow; Fuel cell

1. Introduction

Increasing societal demand for a wide range of small, often portable devices capable of operating for extended periods without recharging has resulted in a surge of research in the development of micro power sources [1–3]. These portable applications include not only common appliances such as cell phones, laptop computers, and personal organizers, but also more specialized devices such as clinical and diagnostic tests, microanalytical systems for field tests, and global positioning systems. To date, microscale systems research has focused mostly on miniaturization of functional components, leaving miniaturization of long lifetime power sources as one of the major challenges.

The specific power source studied in this paper is a fuel cell that utilizes a unique property of fluid flow at the microscale, multi-stream laminar flow (Fig. 1). The dimensions and operating conditions of the microfluidic fuel cells discussed here are such that fluid flow is pressure driven and characterized by a Reynolds number, *Re*, less than 10. Two different aqueous streams introduced into the same channel at Re $<\sim$ 2100, will proceed to flow laminarly in parallel as the viscous effects dominate over the inertial effects.

The only remaining mechanism of mixing is diffusion across the mutual liquid–liquid interface between the two streams transverse to the direction of flow. Utilization of this phenomenon in microfluidic systems has recently resulted in a number of interesting applications such as the creation of DNA analysis devices [4], blood diagnostics [5], pH gradients for use in iso-electric focusing [6], vanadium-based redox flow cells [7], microfluidic circuit boards [8], separations [9], in-channel microfabrication [10], and has inspired the development of a laminar flow-based fuel cell [11].

Many current fuel cell designs employ a static physical barrier such as a proton exchange membrane (PEM) to separate the fuels in the anodic and cathodic compartments. While these PEM-type fuel cell designs have great promise to become the power source of choice for some of the applications mentioned above, there are still problems associated with their operation. Fuel cells run more efficiently at higher temperatures due to faster kinetics, however, the PEM then tends to dry out reducing the effectiveness of proton conduction. Water management is an issue since the PEM has to be hydrated at all times in order to facilitate the transport of protons [12]. Another significant problem for PEM-type fuel cells is fuel crossover through the membrane, which results in a mixed potential at the cathode and thereby lowers the cell performance [13]. Despite extensive efforts, these problems still remain major issues preventing PEM-type fuel cells from being applied in wide-scale portable applications [12].

Table 1
Summary of thermodynamic data for different fuels

Fuel	Reaction	n (e)	$-\Delta H°$ (kJ/mol)	$-\Delta G°$ (kJ/mol)	$E_{rev}°$ (V)	Maximum efficiency (%)
Hydrogen	$H_2 + 0.5O_2 \rightarrow H_2O(l)$	2	286	237.3	1.23	82.97
Methanol	$CH_3OH + 1.5O_2 \rightarrow CO_2 + 2H_2O(l)$	6	726.6	702.5	1.21	96.68
Formic acid	$HCOOH + 0.5O_2 \rightarrow CO_2 + H_2O(l)$	2	270.3	285.5	1.48	105.6

Note that maximum efficiencies greater than 100% are theoretically possible since the conversion of energy can not only come from chemical energy stored in the reactants, but can also be absorbed energy from the surroundings and then converted into electrical energy where the enthalpy and Gibbs free energy are related to entropy and temperature.

The liquid–liquid interface between the two streams in the laminar flow-based fuel cells discussed here, as shown in Fig. 2, has certain advantages over static membrane fuel cells. During operation, convective transport dominates over diffusive transport so fuel crossover can be avoided as the amount of diffusion transverse to the direction of flow can be controlled with high precision by variation of the flow rate of the fuel and oxidant streams. Other advantages include eliminating issues with water management (i.e. membrane dry-out) as the 'membrane' in the laminar flow-based fuel cell is a liquid–liquid interface. The flowing streams automatically remove excess water generated in the electrochemical process. In addition, operation at elevated temperatures is not problematic as long as the temperature avoids the boiling point of the fuel solution used. Another physiochemical phenomenon occurring is the formation of deple-
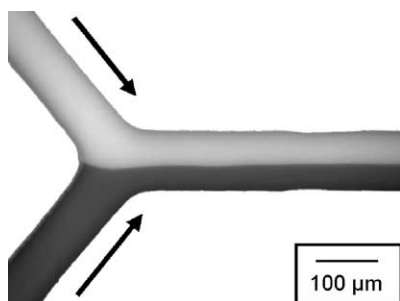

Fig. 1. Optical micrograph of two different dyed aqueous streams flowing in parallel without turbulent mixing.
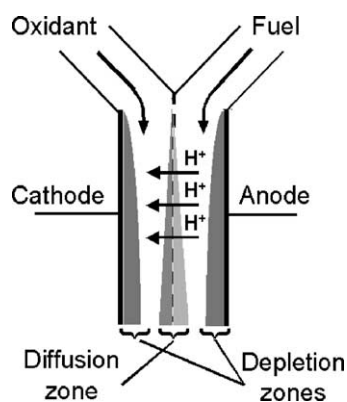

Fig. 2. Schematic of the membraneless laminar flow-based fuel cell. The regions of fuel/oxidant depletion as well as the regions of diffusional fuel/oxidant crossover are indicated (not drawn to scale).

tion boundary layers close to the catalyst-covered electrodes as a result of the reaction of fuel at the anode and oxidant at the cathode (Fig. 2). Adjustments of the flow rates and channel dimensions allow for precise control of the electrochemical processes that take place at the electrodes as will be shown.

Recent catalysis and fuel cell research has indicated that formic acid may be a good alternative to the common fuels of hydrogen and methanol [14,15]. Even though formic acid has a lower energy density than methanol, 7.49 and 17.5 J/ml, respectively, the possibility for a significant increase in performance with the correct catalyst exists [16]. Compared to hydrogen and methanol, formic acid has a higher overall theoretical open circuit potential and maximum efficiency as indicated in Table 1. In sum, formic acid seems to be a promising fuel for fuel cells and thus will be explored as the fuel with the membraneless fuel cell in this paper.

2. Experimental

For all experiments described below, a novel fuel cell consisting of a Y-shaped channel with electrodes on the inner sidewalls of the main channel was manufactured using multiple replication steps. In a typical procedure, a negative of the channel shape, or master, is obtained in thick photoresist (SU-8 series, MicroChem) via standard photolithographic techniques using transparency films as the mask [17]. This master is then replicated into an elastomeric mold, typically in polydimethylsiloxane (PDMS), to obtain a positive relief structure of the microfluidic channels [17]. Subsequently, this mold is replicated to obtain the desired central support structure: a liquid UV-curable adhesive (Norland Optical Adhesive) is applied and spread evenly over the elastomeric mold, then a flat layer of the elastomeric material is applied and clamped on top (i) to level the liquid adhesive, and (ii) to ensure that the top layer touches the top of the positive relief microfluidic channel structure. This clamped assembly is then treated with UV light to cure the liquid adhesive layer. After peeling away the elastomeric top layer and the positive-relief elastomeric mold a freestanding central support structure (0.5–3 mm in thickness) carrying the outlines (sidewalls) of the Y-shaped microfluidic channel system is obtained (Fig. 3).
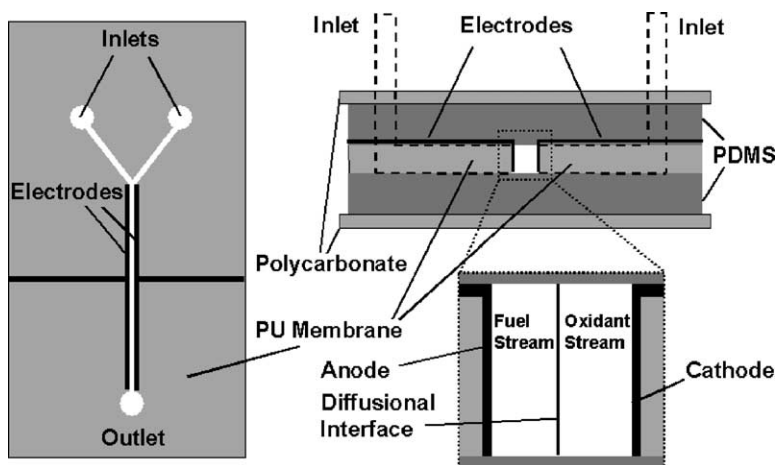
Fig. 3. Stacked assembly of Y-shaped microfluidic membraneless fuel cell system. The inert support structure is a curable polymer, which forms the sidewalls of the Y-shaped channel. These sidewalls carry both the anode and the cathode. A typical channel width is 1000 μm with a height of 1000 μm (not drawn to scale).

The seed layers for the anode and cathode electrodes were applied via sputtering of 25–50 Å of chromium as an adhesion layer followed by 250–1500 Å of gold as the seed layer. Deposition of platinum black catalyst on these seed layers was performed via contact electrodeposition [18].

After applying the appropriate catalyst to the cathode and anode, the central support structure is clamped between two slabs of gasket material, here PDMS typically 1–10 mm in thickness, to form the top and the bottom wall of the Y-shaped microfluidic channel (Fig. 3). More rigid top and bottom capping layers, such as 2 mm-thick pieces of polycarbonate, are applied to provide rigidity and robustness to the layered system.

Polyethylene tubing (Intramedic $Pe = 205$, i.d. 1.57 mm, o.d. 2.08 mm) is placed in one of the two slabs of material to guide the fuel and oxidant into the Y-shaped channel systems and to guide the waste stream out of the channel. The tubing is inserted into holes that are punched exactly at the three ends of the Y-shaped channel design and glued into place. Fluid flow in all of our fuel cell experiments is pressure driven and regulated using a Harvard Apparatus PHD 2000 syringe pump with typical flow rates between 0.3 and 0.8 ml/min per stream.

All experiments were conducted using formic acid (Aldrich 96% ACS grade) or potassium permanganate (Fisher 99.0%) in 18.3 Ω-cm Millipore water as the fuel, and oxygen (S.J. Smith Welding Supply 99.99%) dissolved in 0.5 M sulfuric acid (Fisher Scientific) in 18.3 Ω-cm Millipore water as the oxidant. Oxygen was bubbled through an aqueous solution of 0.5 M sulfuric acid for 15 min with a glass tube ending in a glass frit to aid in the saturation of the solution with oxygen. All experiments were conducted at room temperature with electrodeposited platinum black on both the anode and cathode electrodes as the catalyst. For fuel cell characterization the current and potential were measured at different loads using a variable resistor.

3. Results and discussion

3.1. Physicochemical analysis

The Schmidt and Peclet numbers are dimensionless quantities that allow for the conceptual understanding of the transport issues associated with fluid flow in rectangular ducts similar to the ones studied here. The Schmidt number qualitatively compares molecular diffusivity with momentum diffusivity, $Sc = \nu/D$, where ν is the kinematic viscosity and D is the diffusivity of the species of interest through a particular solvent. Using this scaling analysis, approximate boundary layer thicknesses can be estimated analytically. In our case, the Schmidt number is greater than 1, therefore, the viscous effects diffuse more rapidly than concentration effects exposing the concentration boundary layer to a linear velocity profile. In a typical example, at approximately 100 μm into a channel that has a 1 mm² cross-sectional area at a flow rate of 0.3 ml/min per inlet, the flow is entirely within the viscous boundary layer and the concentration boundary layer is approximately 25 μm thick (Fig. 4).

During multistream laminar flow, diffusion transverse to the direction of flow results in the mixing of the two streams (Fig. 2). The degree of mixing depends on the diffusivities of the species and the time they are in diffusional contact. The Peclet number Pe, is the ratio of diffusive to convective time scales $Pe = UH/D$ where U is average velocity; H, channel height; and D is the diffusivity the species of interest through a particular solvent. By operating the laminar flow fuel cell discussed here at a high Peclet number, typically in the order of 10 000, fuel crossover can be prevented as in this case the convective time scale is shorter than the diffusive time scale [19].

When a heterogeneous reaction occurs at the wall, depletion of the reactant results in formation of a concentration boundary layer or depletion zone which leads to lower conversion rates due to a lower concentration of reactant
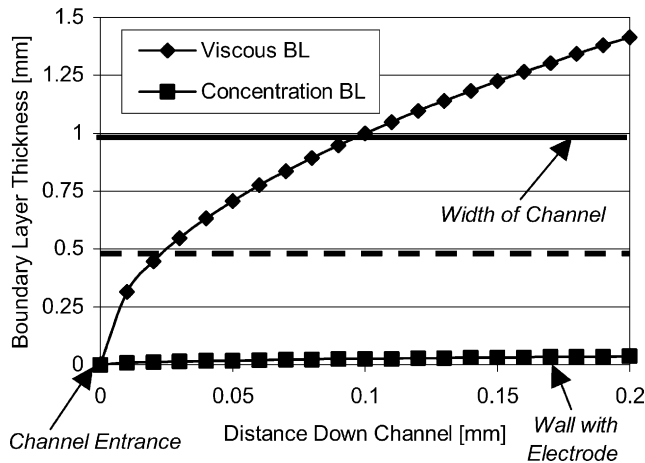
Fig. 4. Viscous and concentration boundary layer growth in the axial direction along the electrode of a 1000 μm × 1000 μm channel based on boundary layer theory.

results in the concentration boundary layer remaining close to the wall and the reactants staying on their original side of the cell.

The performance of the membraneless fuel cell system can be affected by the hydrodynamic stability of the flowing streams. When either the flow is too fast or too slow, deviations from the steady state are observed. At higher flow rates, small hydrodynamic perturbations cause the streams to oscillate, i.e. they vary in relative width, and on occasion touch the opposite electrode. Fuel crossover by diffusion occurs with slower flow rates, resulting in a mixed potential at the cathode and lower cell performance as discussed above. The flow rate operating range of the system varies depending on geometry and composition/concentration of fuel and oxidant streams. The optimum flow rates would, therefore, provide little to no fuel crossover while yielding high fuel and oxidant consumption. Based on experiments studying the dependence of the flow rate on the current, an operating flow rate of 0.5 ml/min was typically used for the fuel cell experiments described below.

3.2. Fuel cell characterization

The performance of the membraneless fuel cell system can be limited by proton conductance due to the distance a proton, generated at the anode, needs to travel to reach the cathode. This resistance limitation can be overcome by adding a proton source such as sulfuric acid to the cathode and/or anode stream, thus providing a supply of protons closer to the cathode while still maintaining a proton gradient due to consumption of protons at the cathode (Fig. 6).

Load curves of the membraneless fuel cell were obtained using 2.1 M formic acid as the fuel and 0.144 M potassium permanganate and oxygen-saturated 0.5 M sulfuric acid as the oxidant in the first and second experiment, respectively. The load curves recorded from these membraneless fuel cells have the same characteristic shape of typical fuel cells with the kinetically limited, ohmic, and mass transport limited regions (Fig. 7). Using the corresponding power density

occupying the region directly next to the electrode than the concentration of the reactant in the bulk region. Therefore, for optimal performance, the concentration boundary layer thickness should be minimized to create a steeper concentration gradient, driving a larger flux of reactants through the depletion region. The system can be modeled as a flat plate and the concentration as a function of time and distance laterally away from the electrode to provide a theoretical representation of the depletion region. This expression can then be used to correlate time with a particular position down the channel to yield a concentration profile for any position in the system as shown in Fig. 5.

By operating at high Peclet and Schmidt numbers (i.e. at $Pe \gg 1$ and $Sc \gg 1$) the concentration boundary layer can be pressed close against the wall and fuel crossover can be prevented simultaneously. The scaling analysis also suggests that reducing the dimensions of the channel will decrease the width of the depletion region while keeping all other process variables constant. Therefore, the best scenario is to utilize small channels having high linear velocities, which
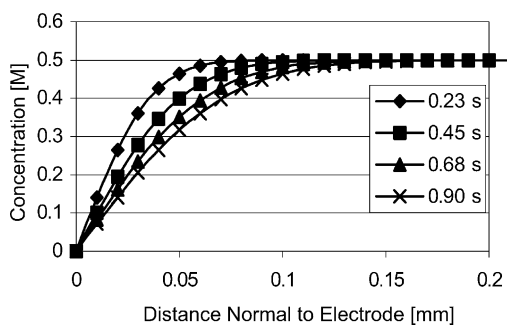

Fig. 5. Depletion region of 0.5 M formic acid bulk concentration normal to the electrode wall at $Pe = 10\,000$ at different residence times modeled using a second order partial differential equation. The position down the length of the channel can be correlated to a residence time in the system by multiplying by the linear velocity.
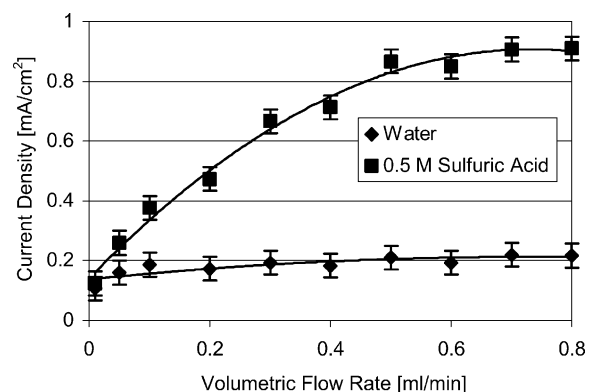

Fig. 6. Current density as a function of volumetric flow rate for experiments performed with 2.1 M formic acid as the fuel and different oxygen saturated oxidant streams.
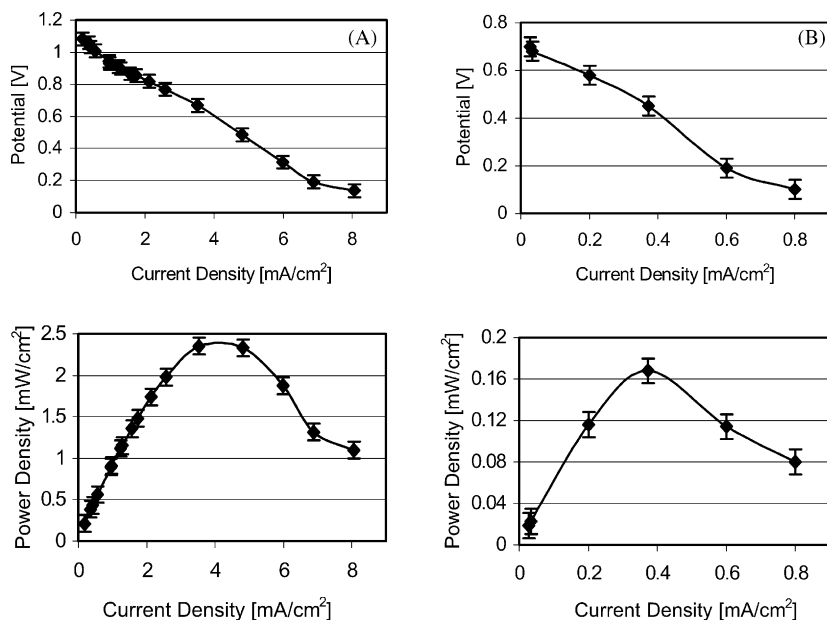
Fig. 7. Load curves and corresponding power density curves of membraneless fuel cells flowing at 0.5 ml/min using 2.1 M formic acid as the fuel and 0.144 M potassium permanganate in 0.5 M sulfuric acid (A) and oxygen saturated 0.5 M sulfuric acid (B) as the oxidant.

curves optimal operation parameters can be deduced: 4.0 and 0.40 mA/cm^2 at potentials of 0.55 and 0.40 V, respectively (Table 2). An order of magnitude higher current density is observed for the system with permanganate instead of oxygen as the oxidant due to the higher oxidant concentration of 144 mM MnO$_4^-$ versus $\sim$0.5 mM of oxygen for the oxygen saturated stream [20].

Formation of bubbles on the electrodes, specifically formation of carbon dioxide bubbles as one of the products of formic acid oxidation at the anode, would hinder the performance of the membraneless fuel cell design by disturbing the flow. However, carbon dioxide has a solubility of 90 ml in 100 ml of water at room temperature and thus the CO$_2$ formed readily dissolves in the flowing stream and is carried out of the system. Bubbles were never observed in our experiments.

The current density did not increase significantly with higher fuel concentrations, which suggests that the performance of the membraneless fuel cells is limited by slow anode/cathode kinetics, low oxidant concentration, or slow diffusion of reagents to the electrode surface due to the formation of a concentration boundary layer. The system, however, cannot be kinetically limited since the current is higher at higher flow rates. Lowering the formic acid concentration to as low as 0.04 M did not result in a reduction of the
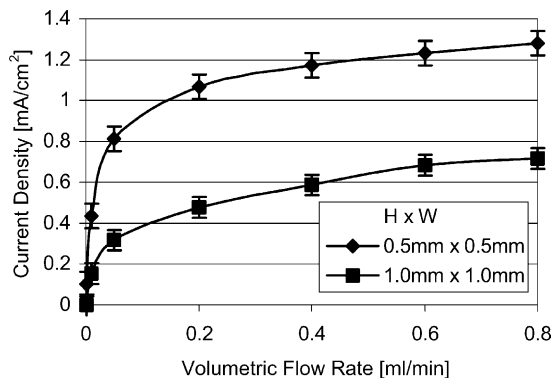

Fig. 8. Current density as a function of volumetric flow rate for different size channels 3.0 cm in length with 1.0 M formic acid as fuel and a 0.5 M sulfuric acid solution saturated with oxygen as the oxidant.

cell's performance, which indicates that the cell is cathode limited. The cathode limitation was confirmed by independent analysis of the anode and cathode using an external reference electrode [21].

The depletion model described in Section 1 above suggests that by reducing the width dimension of the channel will decrease the width of the depletion region with other experimental parameters being constant. Fig. 8 compares the performance of two cells both with 3 cm long channels

Table 2
Summary of performance characteristics of the laminar flow fuel cell experiments shown in Fig. 7

Fuel cathode	Fuel anode	Catalyst	Potential (V)	Current density (mA/cm^2)	Electrochemical efficiency (%)
10% HCOOH	O$_2$/H$_2$SO$_4$	Pt-black	0.4	0.4	27
10% HCOOH	KMnO$_4$	Pt-black	0.55	4	32

The electrochemical efficiencies were calculated by dividing the measured potential by the maximum achievable potential.

but having, respectively, a 1000 μm × 1000 μm (like before) and a 500 μm × 500 μm cross-sectional area. The reduction in size increases the current density at the same volumetric flow rate as suggested by the model. Therefore, by minimizing the concentration boundary layer and having the same bulk concentration, both the flux of fuel and the performance of the cell can be increased. The net result is that one can operate the system at a lower volumetric flow rate in a smaller system to achieve the same performance. This result also leads to the conclusion that the process is diffusion limited and the concentration boundary layer results in a large resistance to reactant transport to the electrodes.

Under the current cell geometry and operating conditions fuel utilization is less than 1.0%. The formation of depletion boundary layers that are not replenished quickly on the electrodes and the excess of fuel that never reaches the electrode surface account for this low conversion rate. As we have observed experimentally, narrowing the channel will increase the fuel efficiency by reducing the width of the boundary layer and minimizing the amount of unreacted fuel passing through the system. Adding a third stream containing only electrolyte between the fuel and oxidant streams could also enhance the conversion efficiency by forcing the fuel stream to be close in size to the concentration boundary layer thickness, approximately 100 μm in the studied system. By operating the system with 0.01 M formic acid, a third stream of only electrolyte 300 μm wide, and a 500 μm × 500 μm cross-sectional channel, it is possible to achieve approximately 65% fuel conversion at the same volumetric flow rate. Other changes to the design of the present membraneless fuel cell prototypes need to be incorporated in order to increase fuel efficiency further.

4. Conclusions

Our results demonstrate the operation of a fuel cell based on multi-stream laminar flow. The present prototypes have electrode areas of 0.15 and 0.3 cm^2 and achievable current densities up to 8 mA/cm^2. The desired goal is to design a device that is optimized with minimal size and maximal current density with significantly high fuel efficiency. New designs will seek to exploit the characteristic advantages of this membraneless system. The current membraneless design possesses a flowing liquid membrane with high ionic conductance, no prominent water management issues, facile product removal, and precise control over fuel crossover. Removal of the membrane results in no membrane "dry-out", a higher temperature tolerance, no maintenance of the membrane, and therefore, reduces the complexity of the fuel cell design.

With the understanding of transport phenomena and operation of the laminar flow-based microfuel cell, strides can be made toward the design of a high performance laminar flow-based microfuel cell. By integrating bi-metallic catalysts, one can improve the performance of methanol and formic acid oxidation, mainly by reducing the amount of CO poisoning of the catalyst. In the methanol case, a platinum/ruthenium catalyst has been shown to improve performance, while in the formic acid case a platinum/palladium catalyst improves performance. Therefore, in future work, integration of these bi-metallic catalysts should dramatically enhance the performance of the currently discussed laminar flow-based micro fuel cell.

Preliminary results suggest that the fuel cell performance is limited by the transport of reactants through the concentration boundary layer to the electrodes and by the low concentration of oxidant in the cathode stream. Through the use of solvents with high oxygen adsorption capability yet good ionic conductivity and new channel designs, improvement in the performance is expected.

The existing fabrication procedure needs to be revised in order to achieve miniaturization of the system. The freestanding inert channel support structure is unmanageable, once its thickness is below 500 μm. Also the use of materials other than PDMS and polyurethane is advisable due to limited compatibility with the fuel and oxidant streams over long periods of time.

Fuel cells receive a lot of attention as potential power sources for a wide variety of applications. While the novel concept discussed in this paper is promising, it is unclear whether this concept is a viable option for practical applications. Issues with parasitic losses due to the need to pump fluids, fuel conversion efficiency, and the potential need to re-circulate the carrier fluid (acidic water) need to be sorted out before a detailed comparison can be made with other fuel cell systems such as those based on PEM membranes.

Acknowledgements

References

[1] A.S. Patil, R. Jacobs, Aerospace and Electronics Systems Magazine, March 2000, pp. 35–37.
[2] A. Jansen, S. van Leeuwen, A. Stevels, IEEE Int. Symp. Electron. Environ. (2000) 155–160.
[3] W.Y. Sim, G.Y. Kim, S.S. Yang, IEEE MEMS (2001) 341–344.
[4] M.A. Burns, B.N. Johnson, S.N. Brahmasandra, K. Handique, J.R. Webster, M.K.T.S. Sammarco, P.M. Man, D. Jones, D. Heldsinger, C.H. Mastrangelo, D.T. Burke, Science 282 (1998) 484–487.
[5] B.H. Wiegl, J. Kriebel, K.J. Mayes, T. Bui, P. Yager, Mikrochim. Acta 131 (1999) 75–83.
[6] K. Macounova, C.R. Cabrera, M.R. Holl, P. Yager, Anal. Chem. 72 (2000) 3745–3751.

[7] R. Ferrigno, A.D. Stroock, T.D. Clark, M. Mayer, G.M. Whitesides, J. Am. Chem. Soc. 124 (2002) 12930–12931.

[8] C.G.J. Schabmueller, M. Koch, A.G.R. Evans, A. Brunnschweiler, J. Micromech. Microeng. 9 (1999) 176–179.

[9] K. Macounova, C.R. Cabrera, P. Yager, Anal. Chem. 73 (2001) 1627–1633.

[10] P.J.A. Kenis, R.F. Ismagilov, G.M. Whitesides, Science 285 (1999) 83–85.

[11] E.R. Choban, L.J. Markoski, J. Stoltzfus, J.S. Moore, P.J.A. Kenis, Power Sources Proc. 40 (2002) 317–320.

[12] L. Carrette, K.A. Friedrich, U. Stimming, Chem. Phys. Chem. 1 (2000) 162–193.

[13] M. Eikerling, A.A. Kornyshev, A.M. Kuznetsov, J. Ulstrup, S. Walbran, J. Phys. Chem. B 105 (2001) 3646–3662.

[14] M. Weber, J.-T. Wang, S. Wasmus, R.F. Savinell, J. Electrochem. Soc. 143 (1996) 158–160.

[15] C. Rice, S. Ha, R.I. Masel, P. Waszczuk, A. Wieckowski, T. Barnard, J. Power Sources 111 (2002) 83–89.

[16] G.-Q. Lu, A. Crown, A. Wieckowski, J. Phys. Chem. 103 (1999) 9700–9711.

[17] D.C. Duffy, J.C. McDonald, O.J.A. Schueller, G.M. Whitesides, Anal. Chem. 70 (1998) 4974–4984.

[18] M.P. Maher, J. Pine, J. Wright, Y. Tai, J. Neur. Methods 87 (1999) 45–56.

[19] R.F. Ismagilov, A.D. Stroock, P.J.A. Kenis, G.M. Whitesides, H.A. Stone, Appl. Phys. Lett. 76 (2000) 2376–2378.

[20] For the solubility of oxygen in aqueous media, see for example: http://www.colby.edu/chemistry/CH331/O2%20Solubility.html.

[21] E.R. Choban, P. Waszczuk, P.J.A. Kenis, Method for Direct Evaluation of Working/Counter Electrode Performance in Microfluidic Electrochemical Systems, manuscript in preparation.